

Benneshierite, $\text{Ba}_2\text{Fe}^{2+}\text{Si}_2\text{O}_7$: A new melilite group mineral from the Hatrurim Basin, Negev Desert, Israel

ARKADIUSZ KRZĄTAŁA^{1,*}, BILJANA KRÜGER², IRINA GALUSKINA¹, YEVGENY VAPNIK³, AND
EVGENY GALUSKIN¹

¹Institute of Earth Sciences, Faculty of Natural Sciences, University of Silesia, Będzińska 60, 41-200 Sosnowiec, Poland

²Institute of Mineralogy and Petrography, University of Innsbruck, Innrain 52, 6020 Innsbruck, Austria

³Department of Geological and Environmental Sciences, Ben-Gurion University of the Negev, POB 653, Beer-Sheva 84105, Israel

ABSTRACT

The first barium member of the melilite group, benneshierite $\text{Ba}_2\text{Fe}^{2+}\text{Si}_2\text{O}_7$ [$P\bar{4}2_1m$, $Z = 2$, $a = 8.2334(14)$ Å, $c = 5.2854(8)$ Å, $V = 359.29(13)$ Å³], was discovered in thin veins of rankinite paralava within pyrometamorphic gehlenite hornfels at Gurim Anticline, Hatrurim Basin, Negev Desert, Israel. Benneshierite occurs in small intergranular spaces between large crystals of rankinite, gehlenite, and garnet together with other Ba-minerals such as fresnoite, walstromite, zadovite, gurimite, hexacelsian, and celsian. It forms transparent, light yellow to lemon-colored crystals with a white streak and a vitreous luster. They exhibit good cleavage on (001), a brittle tenacity, and a conchoidal fracture. The estimated Mohs hardness is 5. Benneshierite has a melilite-type structure with the layers composed of disilicate $(\text{Si}_2\text{O}_7)^{6-}$ groups and $(\text{Fe}^{2+}\text{O}_4)^{6-}$ tetrahedra, connected by large eightfold-coordinated Ba atoms. In some grains, epitaxial intergrowths of benneshierite and fresnoite are observed. The structure of the fresnoite, $\text{Ba}_2\text{TiO}(\text{Si}_2\text{O}_7)$ with a $P4bm$ space group and unit-cell parameters $a = 8.5262(5)$ Å, $c = 5.2199(4)$ Å, is closely related to the structure of benneshierite. Among all the known minerals of the melilite group, benneshierite has a structure characterized by the lowest misfit degree between the tetrahedral ($T1$ and $T2$ sites) and polyhedral (X -site) layers, as it was shown in both natural and synthetic melilite-type phases.

Keywords: Benneshierite, new mineral, melilite group, crystal structure, Raman, fresnoite, paralava, Hatrurim, Israel

INTRODUCTION

A new mineral of the melilite group, benneshierite, $\text{Ba}_2\text{Fe}^{2+}\text{Si}_2\text{O}_7$ (IMA 2019-068), was found in thin veins of rankinite paralava in gehlenite hornfels of the pyrometamorphic Hatrurim Complex in the Negev Desert, Israel. Paralava with benneshierite was found in the immediate vicinity of Ben Neshier Mount, from which the mineral name derives. This rankinite paralava is a source of several new minerals, among which Ba-bearing minerals are predominant, such as zadovite = $\text{BaCa}_6[(\text{SiO}_4)(\text{PO}_4)](\text{PO}_4)_2\text{F}$; aradite = $\text{BaCa}_6[(\text{SiO}_4)(\text{VO}_4)](\text{VO}_4)_2\text{F}$; hexacelsian = $\text{BaAl}_2\text{Si}_2\text{O}_8$; and gurimite = $\text{Ba}_3(\text{VO}_4)_2$ (Galuskin et al. 2015; Galuskina et al. 2017a).

Benneshierite is the first barium member of the melilite group combining seven OH-free minerals and one OH-bearing (Table 1). In a melilite structure with the general formula $X_2T1[(T2)_2\text{O}_7]$ (Bindi et al. 2001; Table 1), layers composed of eightfold-coordinated cations, where $X = \text{Ca}, \text{Na}, \text{Sr}, \text{K}, \text{Ba}, \square$ (vacancy), intercalate with layers formed by a tetrahedrally coordinated $T1$ and $T2$, where $T1 = \text{Mg}, \text{Al}, \text{Fe}^{2+}, \text{Fe}^{3+}, \text{Be}, \text{Zn}, \text{B}, \text{Si}$; and $T2 = \text{Si}, \text{Al}, \text{B}, \text{Be}$. Two $T2$ tetrahedra are linked and form $(T2)_2\text{O}_7$ dimers.

It should be underlined that very small (~10 μm) mineral grains with the empirical formula $(\text{Ba}_{1.6}\text{Sr}_{0.2}\text{Ca}_{0.2})\text{FeSi}_2\text{O}_7$, i.e., with a chemical composition close to benneshierite, were detected in leucite- and melilite-bearing nephelinite from Nyiragongo in

the Virunga volcanic province, Democratic Republic of Congo (Andersen et al. 2014). These rocks contain the other rare barium sorosilicate—andrémeyerite, $\text{BaFe}_2^{3+}\text{Si}_2\text{O}_7$, composed of the same chemical constituents as benneshierite, but with a different Ba:Fe²⁺ atomic ratio. This different ratio is related to the different structural arrangements of these two phases (Sahama et al. 1973).

Benneshierite has synthetic structural analogs: $\text{Ba}_2\text{MgSi}_2\text{O}_7$ (Shimizu et al. 1995), $\text{Ba}_2\text{CoSi}_2\text{O}_7$ (El Bali and Zavalij 2003), $\text{Ba}_2\text{CuSi}_2\text{O}_7$ (Du et al. 2003), and $\text{Ba}_2\text{MnSi}_2\text{O}_7$ (Sale et al. 2019). Ito and Hafner (1974) also used synthetic $\text{Ba}_2\text{Fe}^{2+}\text{Si}_2\text{O}_7$ as a standard for Mössbauer measurements of gadolinite spectra. Synthetic “barium ferroåkermanite,” $\text{Ba}_2\text{Fe}^{2+}\text{Si}_2\text{O}_7$, was used for the study of the valence changing and structural state of iron during melting experiments with the help of Mössbauer spectroscopy (Bychkov et al. 1992).

In rankinite paralava, benneshierite intergrows with structurally related fresnoite, $\text{Ba}_2\text{TiO}(\text{Si}_2\text{O}_7)$. The main difference between the structures of these minerals is that the $T1$ $(\text{Fe}^{2+}\text{O}_4)^{6-}$ tetrahedron in the tetrahedral layer of the benneshierite structure is replaced by a $(\text{TiO}_5)^{6-}$ tetragonal pyramid in the fresnoite structure (Moore and Louisnathan 1969; Bindi et al. 2006). Fresnoite is a rare mineral discovered in sanbornite-bearing metamorphic rocks from the Rush Creek deposit, eastern Fresno County, California, U.S.A., (Alfors et al. 1965) and later found in several localities (Chukanov et al. 2011; Andersen et al. 2014; Solovova et al. 2006; Peretyazhko et al. 2018).

In this paper, we describe the new mineral benneshierite, as

*E-mail: arkadiusz.krzatala@us.edu.pl. Orcid 0000-0002-6100-3091

TABLE 1. Physical properties of benneshierite and selected minerals of the melilite group

Mineral species	End-member	Crystal data	Density	Optical properties
Benneshierite (this study)	$\text{Ba}_2\text{Fe}^{2+}\text{Si}_2\text{O}_7$	$P4_2/m$ $a = 8.2334(14) \text{ \AA}$ $c = 5.2854(8) \text{ \AA}$	4.27 g/cm ³ (calc)	(–) $n_w = 1.590(2)$ $n_e = 1.575(2)$ (+)
Åkermanite [1,2,3]	$\text{Ca}_2\text{Mg}(\text{Si}_2\text{O}_7)$	$P4_2/m$ $a = 7.8288(8) \text{ \AA}$ $c = 5.0052(5) \text{ \AA}$	2.944 g/cm ³	$n_w = 1.6326$ $n_e = 1.6407$ (–)
Alumoåkermanite [4]	$(\text{Ca},\text{Na})_2(\text{Al},\text{Mg},\text{Fe}^{2+})(\text{Si}_2\text{O}_7)$	$P4_2/m$ $a = 7.7661(4) \text{ \AA}$ $c = 5.0297(4) \text{ \AA}$	2.96(2) g/cm ³	$n_w = 1.635(1)$ $n_e = 1.626(1)$ (–)
Gehlenite [2,5]	$\text{Ca}_2\text{Al}(\text{AlSiO}_7)$	$P4_2/m$ $a = 7.7173 \text{ \AA}$ $c = 5.0860 \text{ \AA}$	3.038 g/cm ³	$n_w = 1.669$ $n_e = 1.658$ (synthetic) (–)
Hardystonite [2,6]	$\text{Ca}_2\text{Zn}(\text{Si}_2\text{O}_7)$	$P4_2/m$ $a = 7.8279(10) \text{ \AA}$ $c = 5.0138(6) \text{ \AA}$	3.39–3.44 g/cm ³	$n_w = 1.669$ $n_e = 1.657$ (–)
Okayamalite [7]	$\text{Ca}_2\text{B}(\text{BSiO}_7)$	$P4_2/m$ $a = 7.116 \text{ \AA}$ $c = 4.815 \text{ \AA}$	3.30 g/cm ³ (calc)	$n_w = 1.700$ $n_e = 1.696$ (+)
Gugiaite [8,9]	$\text{Ca}_2\text{Be}(\text{Si}_2\text{O}_7)$	$P4_2/m$ $a = 7.43 \text{ \AA}$ $c = 5.024 \text{ \AA}$	3.0336 g/cm ³	$n_w = 1.664$ $n_e = 1.672$ (+)
Hydroxylgugiaite [10]	$(\text{Ca},\square)_2(\text{Be},\text{Si})[(\text{Si},\text{Be})_2\text{O}_5(\text{OH})_2]$	$P4_2/m$ $a = 7.4151(2) \text{ \AA}$ $c = 4.9652(1) \text{ \AA}$	2.79 g/cm ³ (calc)	$n_w = 1.622(2)$ $n_e = 1.632(1)$ (+)

Notes: 1 = Swainson et al. (1992); 2 = Anthony et al. (2003); 3 = Medenbach and Shannon (1997); 4 = Wiedenmann et al. (2009); 5 = Louisnathan (1971); 6 = Louisnathan (1969); 7 = Matsubara et al. (1998); 8 = Peng et al. (1962); 9 = Yang et al. (2001); 10 = Grice et al. (2017).

well as provide new data on the composition and structure of the associated fresnoite. A small polished fragment of paralava with several grains of benneshierite has been deposited in the Fersman Mineralogical Museum in Moscow, Russia, with the catalog number 97004. Investigations of the mineral composition, optical properties, Raman spectroscopy, and structure refinement were performed on benneshierite grains from this specimen.

EXPERIMENTAL METHODS

Several small fragments of gehlenite hornfels with rankinite-bearing paralava veins (Fig. 1) are the source of benneshierite and fresnoite grains up to 80 μm in size, which are the main objects of the study.

The morphology and composition of the minerals were studied using optical microscopy, a scanning electron microscope (Phenom XL, Institute of Earth Sciences, University of Silesia), and an electron microprobe analyzer (Cameca SX100, Institute of Geochemistry, Mineralogy, and Petrology, University of Warsaw). Chemical analyses were carried out (WDS-mode, 15 keV, 20 nA, $\sim 1 \mu\text{m}$ beam diameter) using the following lines and standard materials: $\text{NaK}\alpha$ = albite; $\text{SiK}\alpha$, $\text{CaK}\alpha$, $\text{MgK}\alpha$ = diopside; $\text{AlK}\alpha$, $\text{KK}\alpha$ = orthoclase; $\text{ZnK}\alpha$ = ZnAs_2 ; $\text{MnK}\alpha$ = rhodonite; $\text{FeK}\alpha$ = Fe_2O_3 ; BaLa = baryte; SrLa = celestine; $\text{TiK}\alpha$ = TiO_2 .

The Raman spectra of benneshierite and fresnoite were recorded on a WITec α 300 R Confocal Raman Microscope (Institute of Earth Science, University of Silesia, Sosnowiec, Poland) equipped with an air-cooled solid-state laser (532 nm) and a CCD camera operating at -61°C . The laser radiation was coupled to a microscope through a single-mode optical fiber with a diameter of 3.5 μm . A Zeiss LD EC Epiplan-Neofluar DIC-100/0.75 NA objective was used. Raman scattered light was focused on a broadband single-mode fiber with an effective pinhole size of about 30 μm , and a monochromator with a 600 mm^{-1} grating was used. The power of the laser at the sample position was $\sim 40 \text{ mW}$. The integration time of measurement was 5 s with the accumulation of 20 scans and the resolution of 3 cm^{-1} . The monochromator was calibrated using the Raman scattering line of a silicon plate (520.7 cm^{-1}). Spectra processing, such as baseline correction and smoothing, was performed using the SpectraCalc software package GRAMS (Galactic Industries Corporation, New Hampshire, U.S.A.). Band fitting was performed using a Gauss-Lorentz cross-product function, with a minimum number of component bands used for the fitting process.

Single-crystal X-ray studies of benneshierite grain $30 \times 30 \times 20 \mu\text{m}$ in size, were carried out with a STOE IPDS-II diffractometer (two-circle goniometer, image plate detector) with $\text{MoK}\alpha$ radiation ($\lambda = 0.71073 \text{ \AA}$). Data were processed using X-Area software (Stoe and Cie 2002), and full-matrix, least-squares calculations were performed with the program package SHELX-97 (Sheldrick 2008). As a starting model, the structure of the synthetic $\text{Ba}_2\text{MgSi}_2\text{O}_7$ (Shimizu et al. 1995)

was used. Sections of reciprocal space were analyzed, and no additional reflections were observed that would implicate a modulated structure. Experimental data are shown in Online Materials¹ Table OM1. The benneshierite structure was refined to $R_1 = 0.045$, taking into consideration the replacement of Ba/Ca on the X-site and Fe/Mg on the T1-site. The T2 position is fully occupied by Si. The atom coordinates (x , y , z) and equivalent isotropic displacement parameters, as well as anisotropic displacement parameters and selected interatomic distances are given in Online Materials¹ Tables OM2, OM3, and OM4, respectively. The refined chemical formula of benneshierite is $(\text{Ba}_{1.70}\text{Ca}_{0.30})(\text{Fe}_{1.62}\text{Mg}_{0.38})\text{Si}_2\text{O}_7$.

Single-crystal synchrotron radiation diffraction experiments on a fresnoite grain ($30 \times 20 \times 20 \mu\text{m}$ in size), separated from intergrowths with benneshierite, were performed at the X06DA beamline at the Swiss Light Source (Paul Scherrer Institute, Villigen, Switzerland). The beamline was equipped with a PILATUS 2M-F detector. The radiation source was an SLS super-bending magnet (2.9 T). A wavelength of $\lambda = 0.70848 \text{ \AA}$ was obtained by using a Bartels monochromator. The detector was placed 90 mm from the sample, with a vertical offset of 60 mm,

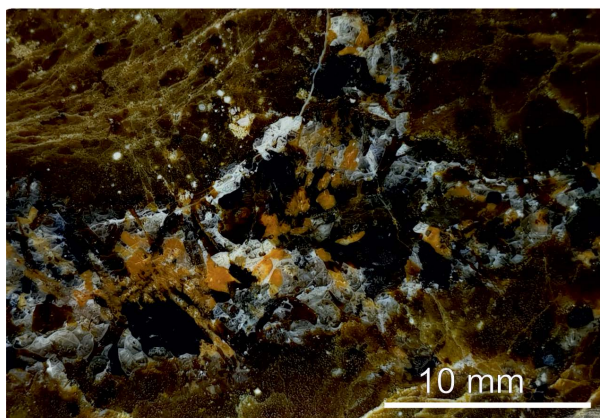


FIGURE 1. Veins of coarse-grained andradite-gehlenite-rankinite paralava within gehlenite hornfels from the Gurim Anticline. The main minerals of this paralava are distinguished by their color: andradite enriched with titanium is black; the melilite of the gehlenite-alumoåkermanite series is brown to yellow-brown; rankinite, fluorapatite, kalsilite, and cuspidine are light-brown, pink, light-gray, or colorless; secondary Ca-hydrosilicates are chalk white.

resulting in a maximum resolution of 0.7 Å. A total of 1800 frames were recorded using a fine-sliced (0.1°) ω -scan at 0.1 s per frame. Lattice parameters were determined using CrysAlisPro (Agilent 2014), whereas the data reduction was processed with XDS (Kabsch 2010). The fresnoite structure was refined to $R_1 = 0.019$, starting from the known fresnoite structure model (Moore and Louisnathan 1967). Experimental details are given in Online Materials¹ Table OM5. The atom coordinates and equivalent isotropic displacement parameters are presented in Online Materials¹ Table OM6, as well as the anisotropic displacement parameters in Online Materials¹ Table OM7 and selected interatomic distances in Online Materials¹ Table OM8. The T1 and T2 sites are fully occupied by Ti and Si, respectively. The refined chemical formula of fresnoite is $(\text{Ba}_{1.94}\text{Ca}_{0.06})\text{TiO}(\text{Si}_2\text{O}_7)$.

OCCURRENCE AND DESCRIPTION OF BENNESHERITE

Bennesherite was discovered in the small veins of coarse-grained andradite-rankinite paralava (Fig. 1) within gehlenite-larnite hornfels found at the Gurim Anticline in the Hatrurim Complex (Mottled zone), Negev Desert, Israel (Krzętała et al. 2020). The type locality (N $31^\circ 12.5'$ E $35^\circ 15.7'$) is situated near Arad city, in the central part of the biggest pyrometamorphic rock area in Israel, named the Hatrurim Basin (Gross 1977; Burg et al. 1991, 1999; Vapnik et al. 2006; Novikov et al. 2013). The rocks of the complex, represented mainly by spurrite marbles, larnite conglomerates and gehlenite hornfels, are distributed along the Dead Sea rift in the territories of Israel, Palestine, and Jordan (Bentor et al. 1963; Gross 1977; Novikov et al. 2013). Scientists generally accept that the terrigenous-carbonate protolith of the Hatrurim Complex was subjected to combustion processes, but the origin of the complex is still debated. The geology and genetic hypotheses of the Hatrurim Complex have already been discussed in some detail (Bentor et al. 1963, 1981; Gross 1977; Minster et al. 1997; Vapnik et al. 2007; Sokol et al. 2010, 2012; Novikov et al. 2013; Galuskina et al. 2014).

The presence of paralava veins in gehlenite hornfels suggests that local pyrometamorphic processes had to be very intense, causing partial or bulk melting of the protolith. The melt crystallization can be confirmed by the presence of eutectic intergrowths of schorlomite-andradite or gehlenite with flamite, as well as walstromite with kalsilite, in the paralava (Gfeller et al. 2015a; Krzętała et al. 2020). The presence of pseudowollastonite in some coarse-grained paralavas clearly suggests that these rocks crystallized from the melt at temperatures of at least 1125°C (Seryotkin et al. 2012). Additionally, coarse-grained rock-forming minerals of paralava (garnet, melilite, rankinite, fluorapatite, and wollastonite) contain melt inclusions with a recorded homogenization temperature of 1200 – 1250°C (Sharygin et al. 2006).

The studied andradite-rankinite paralava from the Gurim Anticline is mainly composed of garnet of the andradite-schorlomite series, melilite of the gehlenite-alumoåkermanite series, rankinite, and fluorapatite. The minor minerals are wollastonite, flamite, and kalsilite. Hematite, members of the magnesioferrite-magnetite series and zadovite-aradite series, walstromite, cuspidine, fresnoite, native copper, gurimite, celsian, hexacelsian, perovskite, combeite-like phase, vorlanite, chalcocite, chalcopyrite, and a heazlewoodite-like mineral are accessory minerals. The secondary minerals are represented by zeolites, tacharanite, afwillite, and tobermorite-like Ca-hydrosilicates.

Bennesherite is a very rare mineral and together with fresnoite occurs in small intergranular spaces between rock-forming minerals associated with other barium minerals such as gurimite, walstromite, hexacelsian or celsian, zadovite, and baryte (Fig. 2).

TABLE 2. Chemical compositions (in wt%) of bennesherite and fresnoite from the Gurim Anticline, Israel

	Bennesherite			Fresnoite		
	Mean	S.D.	Range	Mean	S.D.	Range
	n = 11			n = 10		
SiO_2	25.10	0.40	24.35–25.75	23.82	0.15	23.56–24.09
TiO_2	–	–	–	15.55	0.55	14.50–16.18
Fe_2O_3	0.07 ^a	–	–	0.90	0.46	0.28–1.77
Al_2O_3	0.55	0.07	0.44–0.67	0.38	0.03	0.32–0.41
BaO	55.23	1.35	51.35–56.38	58.64	0.24	58.30–59.01
SrO	0.93	0.27	0.50–1.65	–	–	–
ZnO	0.26	0.05	0.18–0.35	–	–	–
FeO	12.21	0.95	10.88–13.81	–	–	–
MnO	0.28	0.09	0.21–0.46	–	–	–
CaO	2.95	0.61	2.41–4.40	0.45	0.12	0.19–0.62
MgO	0.74	0.19	0.45–1.10	–	–	–
K_2O	0.16	0.03	0.11–0.21	–	–	–
Na_2O	0.17	0.03	0.13–0.22	0.11	0.02	0.08–0.13
Total	98.66	–	–	99.85	–	–
Calculated on 7 O atoms						
Ba^{2+}	1.706	–	–	1.909	–	–
Ca^{2+}	0.249	–	–	0.037	–	–
Sr^{2+}	0.042	–	–	–	–	–
Na^+	0.026	–	–	0.018	–	–
K^+	0.016	–	–	–	–	–
Sum X	2.040	–	–	1.964	–	–
Fe^{2+}	0.774	–	–	0.056	–	–
Ti^{4+}	–	–	–	0.972	–	–
Mg^{2+}	0.087	–	–	–	–	–
Al^{3+}	0.051	–	–	–	–	–
Mn^{2+}	0.019	–	–	–	–	–
Zn^{2+}	0.015	–	–	–	–	–
Fe^{3+}	0.035	–	–	–	–	–
Sum T1	0.982	–	–	1.028	–	–
Si^{4+}	1.978	–	–	1.979	–	–
Al^{3+}	–	–	–	0.037	–	–
Sum T2	1.978	–	–	2.026	–	–

Note: n = number of analyses; S.D. = 1σ = standard deviation. ^a Calculated on charge balance.

Particularly conspicuous is the fact that fresnoite occurs as a more stable mineral and does not exhibit an imprint of low-temperature alteration, where nearby bennesherite grains show edges substituted by late hydrosilicates (Fig. 2b). Sometimes epitaxial intergrowths of bennesherite and fresnoite are observed (Fig. 2d).

The bennesherite crystals, up to $80\ \mu\text{m}$ long, exhibit a light yellow to lemon color and a white streak. The crystals are transparent and have a vitreous luster. They are characterized by good cleavage on (001). Parting is not observed, tenacity is brittle, and fracture is conchoidal. Bennesherite is uniaxial (–) with refractive indices ($589\ \text{nm}$) $n_\omega = 1.711(2)$, $n_e = 1.708(2)$. The calculated density, based on the average chemical composition and unit-cell parameters, is $4.39\ \text{g/cm}^3$. Micro-hardness measurements gave a mean VHN_{25} value of $540\ \text{kg/mm}^2$ (ranging from 527 to $565\ \text{kg/mm}^2$) based on 12 measurements. This value corresponds to a Mohs hardness of ca. 5.

The chemical data for bennesherite from the Gurim Anticline are presented in Table 2. The empirical formula calculated on the basis of seven oxygen atoms per formula unit is $(\text{Ba}_{1.706}\text{Ca}_{0.249}\text{Sr}_{0.042}\text{Na}_{0.026}\text{K}_{0.016})_{\Sigma 2.040}(\text{Fe}_{0.774}\text{Mg}_{0.087}\text{Al}_{0.051}\text{Fe}_{0.035}\text{Mn}_{0.019}\text{Zn}_{0.015})_{\Sigma 0.982}\text{Si}_{1.978}\text{O}_7$ and can be simplified to $\text{Ba}_2\text{Fe}^{2+}(\text{Si}_2\text{O}_7)$. Bennesherite shows a relatively constant composition, with the highest variations observed in the number of minor elements like Ca, Sr, and Mg (Table 2).

Fresnoite associated with bennesherite forms crystals with a more intense yellow color than bennesherite. Its crystals reach $40\ \mu\text{m}$ in size. Fresnoite is characterized by a constant composition (Table 2). The empirical formula of the investigated crystals is as follows: $(\text{Ba}_{1.90}\text{Ca}_{0.04}\text{Na}_{0.02})_{\Sigma 1.96}(\text{Ti}_{0.97}\text{Fe}_{0.06})_{\Sigma 1.03}[(\text{Si}_{1.97}\text{Al}_{0.04})_{\Sigma 2.01}\text{O}_7]\text{O}$.

Raman investigation

The Raman spectrum of benneshierite (Fig. 3a) differs significantly from the spectra of the melilite group minerals and their synthetic analogs in the 500–800 cm^{-1} range (Sharma et al. 1983; Bouhifd et al. 2002; Hanuza et al. 2012). In the benneshierite spectrum, bands observed in the 890–1060 cm^{-1} range correspond to stretching antisymmetric $\nu_{\text{as}}(\text{Si-O-Si})$ and symmetric $\nu_{\text{s}}(\text{SiO}_3)$ vibrations (Sharma et al. 1983): 1015 cm^{-1} $\nu_{\text{as}}(\text{Si-O-Si})$; 970 and 912 cm^{-1} $\nu_{\text{s}}(\text{SiO}_3)$. The bands in the range from 370 to 860 cm^{-1} are strongly coupled, and the majority exhibit a mixed nature. These appear in the Raman spectra of both benneshierite and other melilite-related phases (Hanuza et al. 2012). A shoulder at 823 cm^{-1} is interpreted as the vibration modes of $\nu_{\text{as}}(\text{SiO}_3) + \gamma(\text{Si-O-Si})$ (out-of-plane vibrations of the bridge). The bands at 702 and 669 cm^{-1} are determined by the $\nu_{\text{s}}(\text{Si-O-Si}) + \nu_{\text{s}}(\text{SiO}_3)$ vibrations, and the bands at 635, 611, 585, and 563 cm^{-1} are connected with bending $\delta_{\text{s}}(\text{SiO}_3) + \text{translation } T'(\text{Ba}^{2+}) + \text{stretching } \nu_{\text{s}}(\text{Fe}^{2+}\text{O}_4)^{6-}$ vibrations (Fig. 3a). The stretching vibrations of $\nu_{\text{s}}(\text{Fe}^{2+}\text{O}_4)^{6-}$ are probably the main contribution to the band at 585 cm^{-1} . For comparison, in eltyubyuite, $\text{Ca}_{12}\text{Fe}_{10}^{3+}\text{Si}_4\text{O}_{32}\text{Cl}_2$, the band from $\nu_{\text{s}}(\text{Fe}^{3+}\text{O}_4)^{5-}$ vibrations is at about 730 cm^{-1} (Gfeller et al. 2015b). The bands at 469, 434, and 411 cm^{-1} in the benneshierite Raman spectrum correspond to the bending vibrations of $\delta_{\text{as}}(\text{SiO}_3) + \delta(\text{Si-O-Si})$ (in-plane vibrations of the bridge), with a likely contribution from $T'(\text{Ba}^{2+}) + T'(\text{Fe}^{2+})$ vibrations. In the lower

range, the band at 308 cm^{-1} is mainly related to $\rho(\text{SiO}_3)$ (rocking vibrations), whereas the band at 272 cm^{-1} is related to $\delta(\text{Si-O-Si})$ vibrations (Hanuza et al. 2012). The broad band, centered near

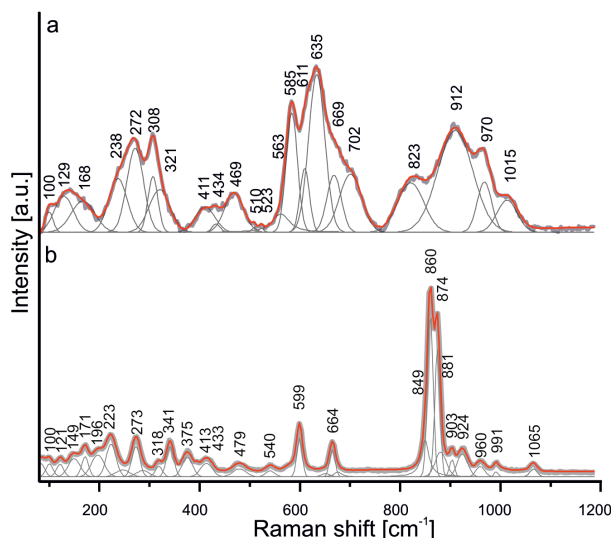
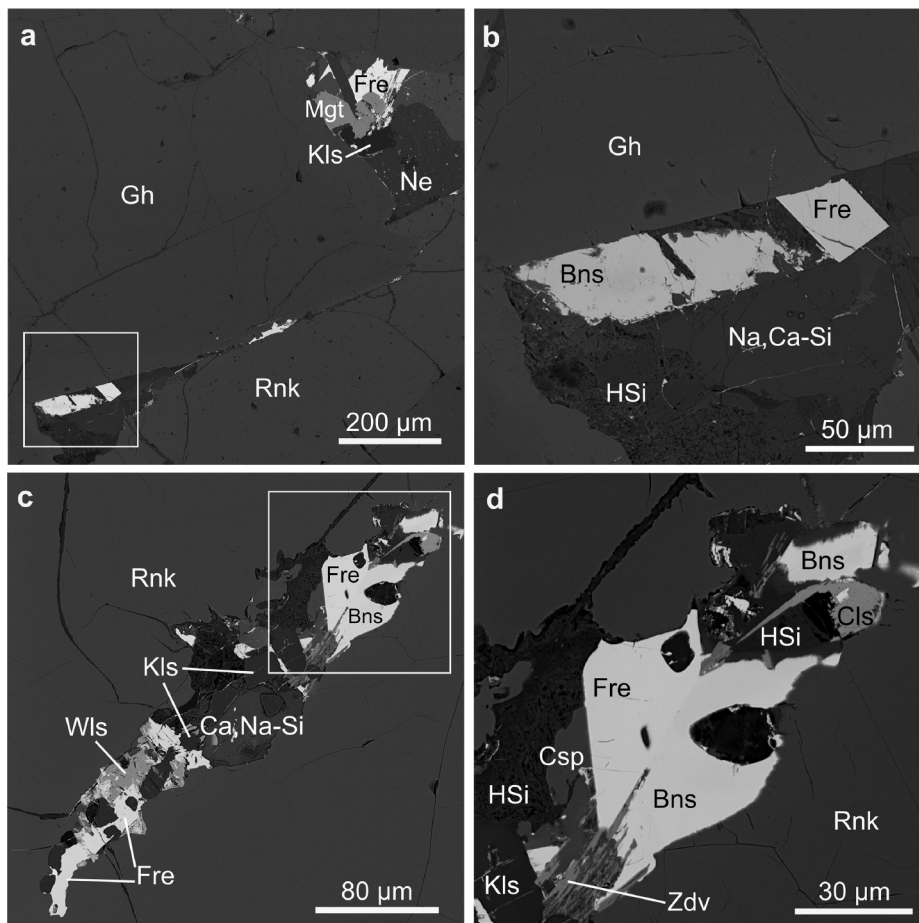


FIGURE 3. Raman spectra of (a) benneshierite, $\text{Ba}_2\text{Fe}^{2+}\text{Si}_2\text{O}_7$ and (b) fresnoite, $\text{Ba}_2\text{TiO}(\text{Si}_2\text{O}_7)$ in paralava from the Hatrum Complex.

FIGURE 2. Backscattered electron (BSE) images of benneshierite in paralava from the Gurim Anticline: (a) Crystals of benneshierite occur between rock-forming minerals, the frames point out the magnified fragment shown in b. (b) Benneshierite in association with fresnoite. (c and d) Benneshierite in small cavities within the rankinite crystals together with other barium minerals such as fresnoite, walstromite, celsian, or zadovite. The framed fragment is magnified and shown in d. Labels: Bns = benneshierite, Cls = celsian, Csp = cuspidine, Fre = fresnoite, Gh = gehlenite, HSi = hydrosilicate of calcium, Kls = kalsilite, Mgt = magnetite, Rnk = rankinite, Wls = walstromite, Zdv = zadovite.



128 cm^{-1} , is ascribed to Ba–O vibrations.

The Raman spectrum of fresnoite (Fig. 3b) associated with benneshierite is distinguished from the spectra of the melilite group minerals and is similar to the fresnoite spectra presented by other authors (Blasse 1979; Gabelica-Robert and Tarte 1981). The strong bands in the spectrum of Israeli fresnoite, at 860 and 874 cm^{-1} , have a complex nature. They are defined by $\nu_3(\text{SiO}_3)$ vibrations in $(\text{Si}_2\text{O}_7)^{6-}$ and $\nu(\text{Ti-O}_{\text{ap}})$ vibrations in the $(\text{TiO}_5)^{6-}$ tetragonal pyramid (Gabelica-Robert and Tarte 1981), in which the apical oxygen is spaced at an anomalously short distance $\text{Ti-O}_{\text{ap}} \approx 1.69\text{ Å}$ (see description of the structure below). The band at 664 cm^{-1} is related to stretching vibrations $\nu_3(\text{Si-O-Si})$, and the bands at 599 , 341 , and 273 cm^{-1} are connected with bending $\delta(\text{SiO}_3)$ and $\delta(\text{Si-O-Si})$ vibrations in $(\text{Si}_2\text{O}_7)^{6-}$ (Gabelica-Robert and Tarte 1981).

Single-crystal data of benneshierite and associated fresnoite

Benneshierite, $\text{Ba}_2\text{Fe}^{2+}\text{Si}_2\text{O}_7$, with a $P4_2/m$ space group and $a = 8.2334(14)\text{ Å}$, $c = 5.2854(8)\text{ Å}$ cell parameters is isostructural with sorosilicates of the melilite group with the general formula $X_2\text{Tl}[(\text{T}_2\text{O}_7)]$ (Bindi et al. 2001; Table 1). In the benneshierite structure (Figs. 4a–4c; Online Materials¹ Tables OM1–OM4), layers of eightfold-coordinated Ba cations intercalate with layers formed by tetrahedrally coordinated $\text{Tl} = \text{Fe}^{2+}$, Mg, and $\text{T}_2 = \text{Si}$. Two T_2O_4 tetrahedra form (Si_2O_7) dimers. The Ba atom is coordinated by eight O atoms with the bond distance ranging from 2.609 to 2.908 Å and an average Ba–O distance of 2.776 Å (Online Materials¹ Table OM4). The smaller SiO_4 tetrahedra exhibit an average bond distance of 1.632 Å , but they are highly irregular with distances ranging from $1.583(19)$ to $1.651(14)\text{ Å}$ (Online Materials¹ Table OM4). The larger TlO_4 tetrahedra are regular with four equal Tl-O bonds of $1.957(14)\text{ Å}$ and flattened along $[001]$ (Fig. 4b). Researchers have observed this type of deformation of the TlO_4 tetrahedron in other melilite group members (Swainson et al. 1992; Kusaka et al. 1998; Bindi et al. 2001; Hejny et al. 2016). Bond valence sum calculations indicate that the iron in benneshierite is mainly represented by Fe^{2+} (Online Materials¹ Table OM9). No twinning and no additional reflections, which would implicate a modulated structure, were observed in the XRD data of benneshierite.

Still, after the full refinement of the benneshierite structure, two residual electron density maxima can be observed in the difference-Fourier map. The first peak with 2.6 e^- is at $(0\ 0\ 0.1716)$ and 0.91 Å from the Fe1/Mg1 position. The second peak at $(0\ 0\ 0.5)$ is 1.75 e^- high and is at a distance of 2.46 Å from O3 and 2.64 Å to Tl. In our opinion, these additional peaks are contributions from another grain. Sections of reciprocal space showed additional reflections from a second intergrown grain with a slightly different orientation. These reflections are weak but at low angles partially overlap with reflections from the studied crystal. We have also considered the following options and they do not explain the additional peaks:

(1) Part of the grain, maybe some small domain, could have a fresnoite structure (with a fivefold-coordinated Fe1/Mg1 position). Possible intergrowth of this additional “phase” with our structure would not match with the positions of the additional peaks. And the resulting fivefold-coordinated polyhedra would be very deformed with some extra short and extra-long non-meaningful bonds.

(2) Part of the grain (some domain) has a monoclinic structure

($C2/c$, $Z = 4$) like $\text{Ba}_2\text{MgSi}_2\text{O}_7$ (Aitasalo et al. 2006) or $\text{Ba}_2\text{ZnSi}_2\text{O}_7$ (Kaiser and Jeitschko 2002). The overlap of monoclinic and tetragonal “phases” does not correspond to the additional peak positions.

As benneshierite forms oriented intergrowths with fresnoite in rankinite paralava from Israel (Fig. 2d), it was decided to study the structure of the fresnoite (Online Materials¹ Tables OM5–OM8) and compare its structure with that of benneshierite. Fresnoite also crystallizes in a non-centrosymmetric tetragonal system like benneshierite, but in a different space group ($P4bm$). The obtained unit-cell parameters, $a = 8.5262(5)\text{ Å}$, $c = 5.2199(4)\text{ Å}$, are close to the data presented by Alfors (1965). The structure of fresnoite is similar to that of benneshierite (Fig. 4). The main difference is that a Tl site is occupied by Fe^{2+}/Mg in benneshierite and by Ti^{4+} in fresnoite. The Ti atoms have an unusual fivefold coordination at the tetragonal-pyramidal site (Fig. 4f). The Tl1 site is coordinated by five oxygen atoms with four bonds $\text{Ti-O} = 1.971(3)\text{ Å}$ (square), and the anomalously short bond to the apical oxygen (Ti-O_4) is $1.694(7)\text{ Å}$ (Online Materials¹ Table OM8). The Ba-site in fresnoite is coordinated by eight O atoms with the bond distance in the range of 2.653 – 3.003 Å , at an average distance of 2.850 Å . The average Si–O bond distance in SiO_4 tetrahedra is 1.623 Å , with the bonds ranging from 1.592 to 1.660 Å .

DISCUSSION

Currently, eight mineral species are combined in the melilite group: äkermanite, alumoäkermanite, benneshierite, gehlenite, gugiaite, hardystonite, hydroxylgugiaite, and okayamalite (Table 1). In our opinion, the two minerals of the melilite group, alumoäkermanite [IMA 2008-049] and hydroxylgugiaite [IMA 2016-009], do not conform to the CNMNC-IMA requirements because their compositions are not compliant with the end-member formula. Alumoäkermanite, $(\text{Ca},\text{Na})_2(\text{Al},\text{Mg},\text{Fe}^{2+})\text{Si}_2\text{O}_7$, is approved as the mixture of the two end-members in a 50/50 ratio—theoretical “soda-melilite”, $(\text{NaCa})\text{AlSi}_2\text{O}_7$, and gehlenite, $\text{Ca}_2\text{Al}(\text{AlSi})\text{O}_7$ (Wiedenmann et al. 2009; Krz̄ała et al. 2020). Hydroxylgugiaite, $(\text{Ca}_3\text{□})_{24}\text{Si}_2(\text{Be}_{2.5}\text{Si}_{1.5})_{26}\text{O}_{11}(\text{OH})_3$, has more than one site with double-site occupation (Grice et al. 2017).

The theoretical end-members of “ferrogehlenite,” $\text{Ca}_2\text{Fe}^{2+}\text{Si}_2\text{O}_7$, and “ferrigehehlenite,” $\text{Ca}_2\text{Fe}^{3+}\text{AlSiO}_7$, are often used to recalculate the chemical analyses of the melilite group minerals to end-member formulas. We have found a mineral with a chemical composition close to “ferrigehehlenite,” $\approx (\text{Ca}_{1.8}\text{Na}_{0.2})(\text{Fe}_{0.65}^{3+}\text{Al}_{0.35})(\text{Si}_{1.2}\text{Al}_{0.8})\text{O}_7$, in association with khesinite in the schorlomite-rankinite paralava of the Hatrurim Complex. However, further structural investigation resulted in the refined formula $\sim \text{Ca}_{1.8}\text{Na}_{0.2}(\text{Al}_{0.7}\text{Fe}_{0.30})(\text{Si}_{1.2}\text{Al}_{0.45}\text{Fe}_{0.36})\text{O}_7$, showing that Fe atoms in its structure are equally allocated to Tl and T2 sites (our unpublished data). Similar Fe^{3+} distribution was noted for the synthetic phases of the $\text{Ca}_2\text{MgSi}_2\text{O}_7$ – $\text{Ca}_2\text{Fe}^{3+}\text{AlSiO}_7$ series (Hamada and Akasaka 2013). For this reason and that the total ratio of $\text{Al} > \text{Fe}^{3+}$, this “ferrigehehlenite” is formally gehlenite. It is interesting that the “ferrigehehlenite” described from coal-fire buchite from Buffalo, Wyoming, U.S.A. (Foit et al. 1987) turned out to be a khesinite $\text{Ca}_4\text{Mg}_2\text{Fe}_{10}^{3+}\text{O}_4[(\text{Fe}_{10}^{3+}\text{Si}_2)\text{O}_{36}]$, the rhönite group mineral described 30 years later (Galuskina et al. 2017b).

It is necessary to add that, according to the structural hierar-

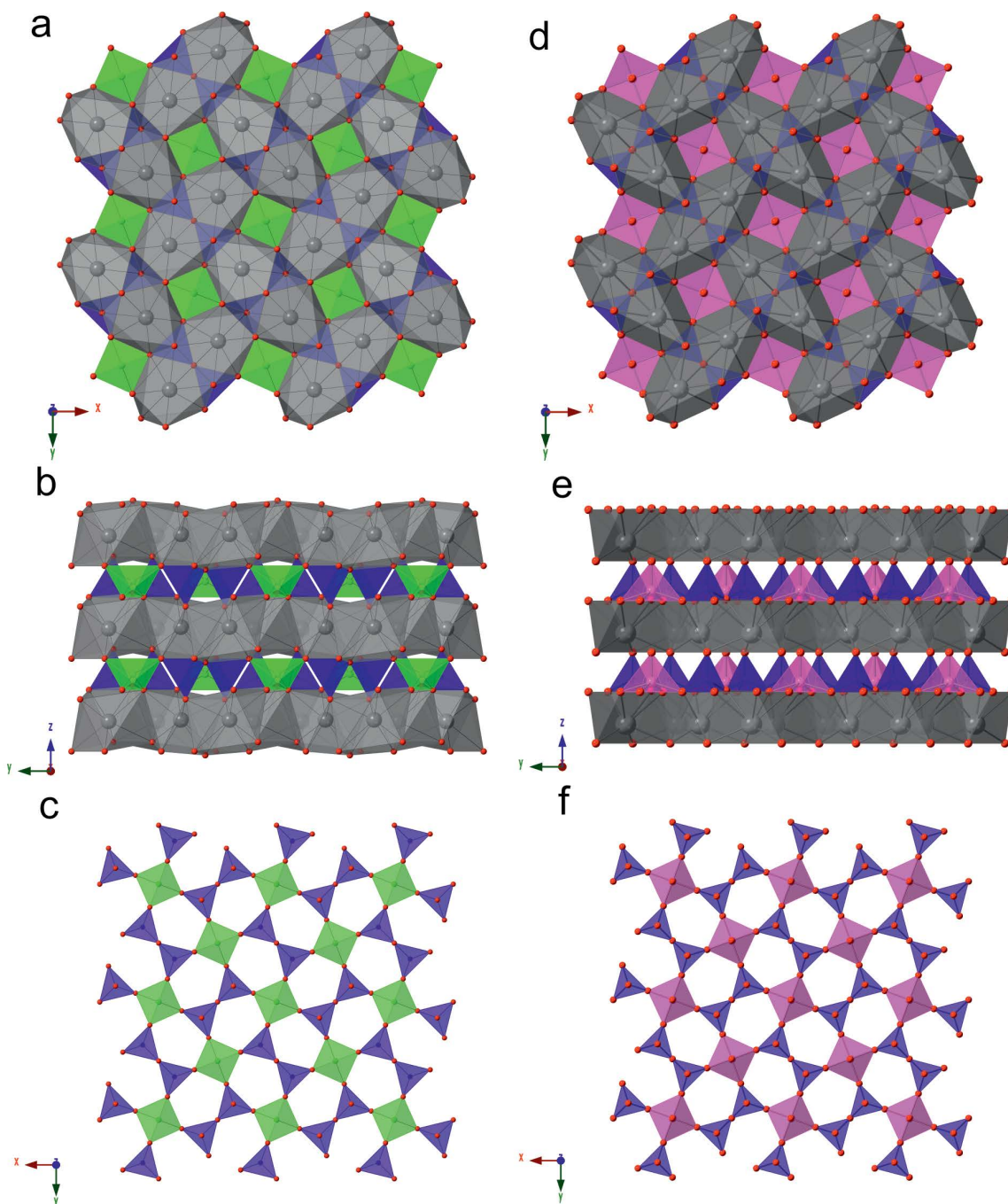


FIGURE 4. The structure of benneshnerite (a, b, and c) and fresnoite (d, e, and f). (a and d) (001) projection; (b and e) tetrahedral layer; (c and f) (100) projection. Ba/Ca-polyhedra (spheres) have a gray color, Fe/Mg-tetrahedra have a green color, Ti-pyramids have a purple color, and Si-tetrahedra have a navy-blue color.

chy of the sheet silicates (Hawthorne et al. 2019), the minerals leucophanite, meliphanite, and jeffreyite have a melilite-related structure. The chemical composition and topology of their sheets are more complex compared to melilite-type minerals (Grice and Robinson 1984; Grice and Hawthorne 1989; Cannillo et al. 1992; Bindi et al. 2003; Lyalina et al. 2019).

Benneshnerite, $\text{Ba}_2\text{Fe}^{2+}\text{Si}_2\text{O}_7$, is the first natural melilite with a big cation at the *X*-site. Geometrical restrictions of the

melilite structure exist in terms of the size of the tetrahedral cations with respect to the size of the interlayer *X* cations. The greater the size of the *T1* and *T2* tetrahedra in comparison with the *X*-site polyhedron (*T/X* ratio), the bigger the internal structural strains between the tetrahedral and polyhedral layers and, as a result, consequent deformation of the tetrahedral layers and structure modulation appear (Seifert et al. 1987; Giuli et al. 2000). In Figure 5, the structural parameters:

$\{T1\text{-}O3\text{-}T2\}^\circ$ angle, tetrahedra angular distortions σ_{T1}^2 and σ_{T2}^2 , calculated for the $T1$ and $T2$ tetrahedra, respectively, according to the formula by Robinson et al. (1971), are plotted against the T/X ratio for several melilite-type compounds. The T/X ratio, calculated as $[(T1\text{-}O)_{\text{mean}} + 2 \cdot (T2\text{-}O)_{\text{mean}}]/3 \cdot (X\text{-}O)_{\text{mean}}$ (Giuli et al. 2000), for benneshierite is equal to 0.627, which is the lowest value among the known melilite group minerals (Fig. 5) and indicates that this mineral shows the least misfit between the tetrahedral and BaO_8 layers. Formerly, okayamalite, $\text{Ca}_2\text{B}_2\text{SiO}_7$, was considered as the mineral with the least T/X parameter (Giuli et al. 2000; Fig. 5). The relatively low misfit of tetrahedral and polyhedral layers in benneshierite, which does not favor the formation of incommensurate modulation of structure, is determined by the big angle $\{T1\text{-}O3\text{-}T2\}^\circ = 125.6^\circ$, the relatively small value of angular distortion of the $T2$ tetrahedron, $\sigma_{T2}^2 = 39.4$, and the high value of angular distortion of the $T1$ tetrahedron, $\sigma_{T1}^2 = 143.5$, in comparison with other minerals of the melilite group (Fig. 5). At the same time, a synthetic Mg-analog of benneshierite, $\text{Ba}_2\text{MgSi}_2\text{O}_6$ (Shimizu et al. 1995), is characterized by a T/X ratio = 0.625 and angle $\{T1\text{-}O3\text{-}T2\}^\circ = 124.6^\circ$, similar to benneshierite, and also by a relatively weaker angular distortion of the tetrahedra: $\sigma_{T1}^2 = 84.1$ and $\sigma_{T2}^2 = 28.2$, respectively. The synthetic phase $\text{Ba}_2\text{CuSi}_2\text{O}_7$, which has a more deformed $T1$ tetrahedron with the highest angular distortion $\sigma_{T1}^2 = 199.7$, is characterized by the lowest T/X ratio = 0.62 (Fig. 5). Replacement of Si by Ge in the $T2$ tetrahedron of Ba-melilites significantly promotes the misfit of the tetrahedral and polyhedral layers, for example, the T/X ratios for $\text{Ba}_2\text{FeGe}_2\text{O}_7$ and $\text{Ba}_2\text{CuGe}_2\text{O}_7$ are 0.65 and 0.647, respectively (Fig. 5). Generally, for melilite-type structures, low values of the T/X ratio cause greater angular distortion of $T1$ and a lower angular distortion of $T2$, and increase the angle $\{T1\text{-}O3\text{-}T2\}^\circ$, which is the most noticeably manifested for Ba-melilites (Fig. 5). In Ba-melilites, the large cation at the X -site defines the $T1$ and $T2$ tetrahedra geometry, influencing the best atomic arrangement to minimize the intrinsic structural strain between the tetrahedral and XO_8 layers. Consequently, in benneshierite, the potential isomorphic replacement of Fe^{2+} by other divalent elements, for example, Mg, Mn^{2+} , Zn, should not cause structural tensions leading to incommensurate modulation.

The genesis of the unusual barium mineralization in the rankinite paralava of the Hatrurim Basin has been previously discussed (Galuskina et al. 2017a; Krz̄ała et al. 2020). Crystallization of the melilite group minerals in rankinite paralava from the Hatrurim Complex has exposed two general trends: in later zones of gehlenite, the Fe^{3+} content increases, whereas in later zones of ākermanite-alumoākermanite minerals, increasing content of Fe^{2+} is noted (Krz̄ała et al. 2020). Generally, the paralava crystallizes from Ca-rich silicate melt. This is indicated by the eutectic structures of flamite + Ti-bearing andradite, flamite + gehlenite, and walstromite + kalsilite (Gfeller et al. 2015a; Sokol et al. 2015; Krz̄ała et al. 2020). Benneshierite and fresnoite are found in small intergranular spaces between the larger crystals of gehlenite, Ti-rich andradite, rankinite, and fluorapatite. Crystallization of relatively large crystals of rock-forming minerals began from cracks in walls forming a solid rock skeleton filled by residual melt. These portions of compositionally inhomogeneous residual melt are the source of material from which later zones of

rock-forming minerals are grown. In the last portions of residual melt, elements incompatible with rock-forming minerals (in these conditions) accumulated and that resulted in the crystallization of diverse minerals containing Ba, V, P, U, S, and Nb (Ga-

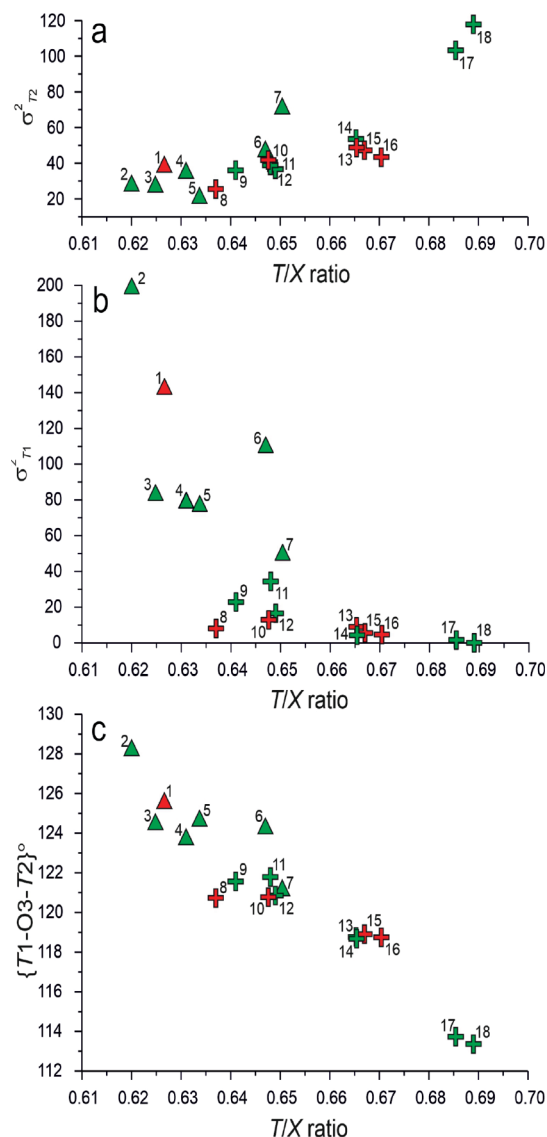


FIGURE 5. (a and b) Values of angular distortion σ^2 calculated according to Robinson et al. (1971) plotted against the T/X ratio. (c) Values of the $\{T1\text{-}O3\text{-}T2\}^\circ$ angle plotted against the T/X ratio. Data used to create the graphs are presented in Online Materials' Table OM10. Symbols: triangle = Ba-melilite; cross = Ba-free melilite; red color = minerals of the melilite group or its synthetic analogs; green color = synthetic phase. 1 = $\text{Ba}_2\text{FeSi}_2\text{O}_7$ (this work); 2 = $\text{Ba}_2\text{CuSi}_2\text{O}_7$ (Du et al. 2003); 3 = $\text{BaMgSi}_2\text{O}_7$ (Shimizu et al. 1995); 4 = $\text{Ba}_2\text{CoSi}_2\text{O}_7$ (El Bali and Zavalij 2003); 5 = $\text{Ba}_2\text{MnSi}_2\text{O}_7$ (Sale et al. 2019); 6 = $\text{Ba}_2\text{CuGe}_2\text{O}_7$ (Tovar et al. 1998); 7 = $\text{Ba}_2\text{FeGe}_2\text{O}_7$ (Malinovskii et al. 1976); 8 = $\text{Ca}_2\text{SiB}_2\text{O}_7$ (Giuli et al. 2000); 9 = $\text{Sr}_2\text{Al}_2\text{SiO}_7$ (Kimata 1984); 10 = $\text{Ca}_2\text{BeSi}_2\text{O}_7$ (Kimata and Ii 1982); 11 = $\text{Sr}_2\text{MgSi}_2\text{O}_7$ (Kimata 1983a); 12 = $(\text{NaCa})\text{AlSi}_2\text{O}_7$ (Louisnathan 1970); 13 = $\text{Ca}_2\text{Al}_2\text{SiO}_7$ (Kimata and Ii 1982); 14 = $\text{Ca}_2\text{CoSi}_2\text{O}_7$ (Kimata 1983b); 15 = $\text{Ca}_2\text{MgSi}_2\text{O}_7$ (Kimata and Ii 1981); 16 = $\text{Ca}_2\text{ZnSi}_2\text{O}_7$ (Louisnathan 1969); 17 = $\text{Y}_2\text{SiBe}_2\text{O}_7$ (Bartram 1969); 18 = $\text{Ca}_2\text{ZnGe}_2\text{O}_7$ (Armbruster et al. 1990).

luskina et al. 2017a; Krzątała et al. 2020). In these small melt portions, conditions for the simultaneous crystallization of benneshierite and fresnoite appeared. The structural similarity of benneshierite and fresnoite (Fig. 4) determines the possibility of their epitaxial intergrowing on (001) (Fig. 2d). The generation of benneshierite growth layers on fresnoite begins on polyhedral layers, as their tetrahedral layers show significant distinctions. In the benneshierite and fresnoite structures, the $(\text{Si}_2\text{O}_7)^{6-}$ dimers are differently oriented. In the fresnoite apices, all SiO_4 -tetrahedra are oriented in the same direction. The bases of the tetrahedra are spread about the same plane $\sim(001)$ and are connected to the corners of the square bases of the $(\text{TiO}_5)^{6-}$ pyramids (Fig. 4). In the same type of layers in the benneshierite structure, the apices of the tetrahedra in the $(\text{Si}_2\text{O}_7)^{6-}$ dimers alternately point to the opposite sides (along the c axis). In this way, the flattened TiO_4 -tetrahedra connect at the edges, with the apices of two dimers pointing up and two pointing down (Fig. 4c).

In conclusion, it can be emphasized that the elasticity of the structure of the melilite group minerals and other minerals with similar structures, for example fresnoite, determines not only their chemical diversity but generates the possibility for an epitaxial intergrowing formation of these minerals.

IMPLICATIONS

Rankinite paralava fills cracks in hornfelses with a mineral composition close to this paralava, and contains minerals, which indicate their crystallization under oxidized conditions, for example, barioferite, $\text{BaFe}_2^{3+}\text{O}_{19}$ (Murashko et al. 2011; Krzątała et al. 2018) or vorlanite $\text{CaU}^{6+}\text{O}_4$ (Galuskin et al. 2013). Small amounts of Fe^{2+} in the minerals of rankinite paralava were detected in the magnesioferite-trevorite-magnetite and äkermanite-gehlenite mineral series (Sharygin et al. 2013; Krzątała et al. 2020). The genesis of the Fe^{2+} -bearing benneshierite in the rankinite paralava in a small portion of residual melt of first cubic millimeters in volume can be connected not only with low-oxygen fugacity and the chemical composition of this melt but also with specific growth effects. Benneshierite, as a rule, forms intergrowths with structurally related fresnoite, which can play the role of a catalyst and an epitaxial substrate for benneshierite nucleation and growth. The crystal chemistry features of benneshierite determine the stabilization of Fe^{2+} in the structure. Thus, in the high-temperature rocks of the Hatrurim Complex, one can expect to find unusual minerals, compositions, and structures, which do not correspond to the general thermodynamic conditions of rock formation because a key role was played by kinetic and crystal chemical factors during their genesis.

FUNDING

This work was supported by the National Science Centre (NCN) of Poland, Grant Preludium No. 2016/21/N/ST10/00463.

REFERENCES CITED

- Agilent (2014) CrysAlis PRO. Agilent Technologies Ltd., Yarmton, Oxfordshire, England.
- Aitasalo, T., Hölsä, J., Laamanen, T., Lastusaari, M., Letho, L., Niittykoski, J., and Pellé, F. (2006) Crystal structure of the monoclinic $\text{Ba}_2\text{MgSi}_2\text{O}_7$: persistent luminescence material. *Zeitschrift für Kristallographie Supplement*, 23, 481–486.
- Alfors, J.T., Stinson, M.C., Matthews, R.A., and Pabst, A. (1965) Seven new barium minerals from eastern Fresno County, California. *American Mineralogist*, 50, 314–340.
- Andersen, T., Elburg, M.A., and Erambert, M. (2014) Extreme peralkalinity in delhayelite- and andremeyerite-bearing nephelinite from Nyiragongo volcano, East African Rift. *Lithos*, 206–207, 164–178.
- Anthony, J.W., Bideaux, R.A., Bladh, K.W., and Nichols, M.C., Eds. (2003) *Handbook of Mineralogy*. Mineralogical Society of America, Chantilly, Virginia.
- Armbruster, T., Röthlisberger, F., and Seifert, F. (1990) Layer topology, stacking variation, and site distortion in melilite-related compounds in the system $\text{CaO-ZnO-GeO}_2\text{-SiO}_2$. *American Mineralogist*, 75, 847–858.
- Bartram, S.F. (1969) Crystal structure of $\text{Y}_2\text{Si}_2\text{Be}_2\text{O}_7$. *Acta Crystallographica*, B25, 791–795.
- Bentor, Y.K., Gross, S., and Heller, L. (1963) High-temperature minerals in non-metamorphosed sediments in Israel. *Nature*, 199, 478–479.
- Bentor, Y.K., Kastner, M., Perlman, I., and Yellin, Y. (1981) Combustion metamorphism of bituminous sediments and the formation of melts of granitic and sedimentary composition. *Geochimica et Cosmochimica Acta*, 45, 2229–2255.
- Bindi, L., Bonazzi, P., Dušek, M., Petříček, V., and Chapuis, G. (2001) Five-dimensional structure refinement of natural melilite, $(\text{Ca}_{1.88}\text{Sr}_{0.01}\text{Na}_{0.08}\text{K}_{0.02})(\text{Mg}_{0.92}\text{Al}_{0.08})(\text{Si}_{1.98}\text{Al}_{0.02})\text{O}_7$. *Acta Crystallographica*, B57, 739–746.
- Bindi, L., Rees, L.H., and Bonazzi, P. (2003) Twinning in natural melilite simulating a fivefold superstructure. *Acta Crystallographica*, B59, 156–158.
- Bindi, L., Dusek, M., Petricek, V., and Bonazzi, P. (2006) Superspace-symmetry determination and multidimensional refinement of the incommensurately modulated structure of natural fresnoite. *Acta Crystallographica*, B62, 1031–1037.
- Blasse, G. (1979) Fresnoite ($\text{Ba}_2\text{TiSi}_2\text{O}_8$): A luminescent compound with a long decay time. *Journal of Inorganic and Nuclear Chemistry*, 41, 639–641.
- Bouhifd, M.A., Gruener, G., Mysen, B.O., and Richet, P. (2002) Premelting and calcium mobility in gehlenite ($\text{Ca}_2\text{Al}_2\text{SiO}_7$) and pseudowollastonite (CaSiO_3). *Physics and Chemistry of Minerals*, 29, 655–662.
- Burg, A., Starinsky, A., Bartov, Y., and Kolodny, Y. (1991) Geology of the Hatrurim formation ("Mottled zone") in the Hatrurim basin. *Israel Journal of Earth Sciences*, 40, 107–124.
- Burg, A., Kolodny, Y., and Lyakhowsky, V. (1999) Hatrurim-2000: The "Mottled Zone" revisited, forty years later. *Israel Journal of Earth Sciences*, 48, 209–223.
- Bychkov, A., Borisov, A., Kharamov, D., Guzova, A., and Urusov, V. (1992) Change of the valent and structural state of iron ions upon melting of barium ferroäkermanite $\text{Ba}_2\text{FeSi}_2\text{O}_7$. *Doklady Akademii Nauk SSSR*, 322, 525–530.
- Cannillo, E., Giuseppetti, G., Mazzi, F., and Tazzoli, V. (1992) The crystal structure of a rare earth bearing leucophanite: $(\text{Ca,RE})\text{CaNa}_2\text{Be}_2\text{Si}_4\text{O}_{12}(\text{F,OH})_2$. *Zeitschrift für Kristallographie—Crystalline Materials*, 202, 71–80.
- Chukanov, N.V., Rastsvetaeva, R.K., Britvin, S.N., Virus, A.A., Belakovskiy, D.I., Pekov, I.V., Aksenov, S.M., and Ternes, B. (2011) Schüllerite, $\text{Ba}_2\text{Na}(\text{Mn,Ca})(\text{Fe}^{2+},\text{Mg,Fe}^{2+})_2\text{Ti}_2(\text{Si}_2\text{O}_7)_2(\text{O,F})_4$, a new mineral species from the Eifel volcanic district, Germany. *Geology of Ore Deposits*, 53, 767–774.
- Du, J., Zeng, H., Song, L., Dong, Z., Ma, H., Guo, G., and Huang, J. (2003) Synthesis and Structure of a New Polymorph $\text{Ba}_2\text{CuSi}_2\text{O}_7$. *Chinese Journal of Structural Chemistry*, 22, 33–36.
- El Bali, B., and Zavalij, P.Y. (2003) Tetragonal form of barium cobalt disilicate, $\text{Ba}_2\text{CoSi}_2\text{O}_7$. *Acta Crystallographica*, E59, i59–i61.
- Foit, F.F., Hooper, R.L., and Rosenberg, P.E. (1987) An unusual pyroxene, melilite, and iron oxide mineral assemblage in a coal-fire buchite from Buffalo, Wyoming. *American Mineralogist*, 72, 137–147.
- Gabelica-Robert, M., and Tarte, P. (1981) Vibrational spectrum of fresnoite ($\text{Ba}_2\text{TiO}_2\text{Si}_2\text{O}_7$) and isostructural compounds. *Physics and Chemistry of Minerals*, 7, 26–30.
- Galuskin, E.V., Kusz, J., Armbruster, T., Galuskina, I.O., Marzec, K., Vapnik, Y., and Murashko, M. (2013) Vorlanite, $(\text{CaU}^{6+})\text{O}_4$, from Jabel Harmun, Palestinian Autonomy, Israel. *American Mineralogist*, 98, 1938–1942.
- Galuskin, E.V., Gfeller, F., Galuskina, I.O., Pakhomova, A., Armbruster, T., Vapnik, Y., Woodyka, R., Dzierzanowski, P., and Murashko, M. (2015) New minerals with a modular structure derived from hatrurite by the pyrometamorphic Hatrurim Complex. Part II. Zadovite, $\text{BaCa}_4[(\text{SiO}_4)(\text{PO}_4)](\text{PO}_4)_2\text{F}$ and aradite, $\text{BaCa}_4[(\text{SiO}_4)(\text{VO}_4)](\text{VO}_4)_2\text{F}$, from paralavas of the Hatrurim Basin, Negev Desert, Israel. *Mineralogical Magazine*, 79, 1073–1087.
- Galuskina, I.O., Vapnik, Y., Lazic, B., Armbruster, T., Murashko, M., and Galuskin, E.V. (2014) Harmunite CaFe_2O_4 : A new mineral from the Jabel Harmun, West Bank, Palestinian Autonomy, Israel. *American Mineralogist*, 99, 965–975.
- Galuskina, I.O., Galuskin, E.V., Vapnik, Y., Prusik, K., Stasiak, M., Dzierzanowski, P., and Murashko, M. (2017a) Gurimite, $\text{Ba}_3(\text{VO}_4)_2$ and hexacelsian, $\text{BaAl}_4\text{Si}_2\text{O}_{18}$ —Two new minerals from schorlomite-rich paralava of the Hatrurim Complex, Negev Desert, Israel. *Mineralogical Magazine*, 81, 1009–1019.
- Galuskina, I.O., Galuskin, E.V., Pakhomova, A.S., Widmer, R., Armbruster, T., Krüger, B., Grew, E.S., Vapnik, Y., Dzierzanowski, P., and Murashko, M. (2017b) Khesinite, $\text{Ca}_4\text{Mg}_2\text{Fe}_2^{3+}\text{O}_{41}[(\text{Fe}_{10}^{3+}\text{Si}_2\text{O}_{16})_2]$, a new rhönite-group (sapphirine supergroup) mineral from the Negev Desert, Israel—Natural analogue of the SFCA phase. *European Journal of Mineralogy*, 29, 101–116.
- Gfeller, F., Srodek, D., Kusz, J., Dulski, M., Gazeev, V., Galuskina, I., Galuskin, E., and Armbruster, T. (2015b) Mayenite supergroup, part IV: Crystal structure and Raman investigation of Al-free eltyubuyite from the Shadil-Khokh volcano, Kel' Plateau, Southern Ossetia, Russia. *European Journal of Mineralogy*, 27, 137–143.
- Gfeller, F., Widmer, R., Krüger, B., Galuskin, E.V., Galuskina, I.O., and Armbruster, T. (2015a) The crystal structure of flamite and its relation to Ca_2SiO_4 polymorphs and nagelschmidite. *European Journal of Mineralogy*, 27, 755–769.
- Giuli, G., Bindi, L., and Bonazzi, P. (2000) Rietveld refinement of okayamalite, $\text{Ca}_2\text{SiB}_2\text{O}_7$: Structural evidence for the B/Si ordered distribution. *American Min-*

- eralogist, 85, 1512–1515.
- Grice, J.D., and Hawthorne, F.C. (1989) Refinement of the crystal structure of leucophanite. *Canadian Mineralogist*, 27, 193–197.
- Grice, J.D., and Robinson, G.W. (1984) Jeffreyite, $(\text{Ca},\text{Na})_2(\text{Be},\text{Al})\text{Si}_2(\text{O},\text{OH})_7$, a new mineral species and its relation to the melilite group. *Canadian Mineralogist*, 22, 443–446.
- Grice, J.D., Kristiansen, R., Friis, H., Rowe, R., Cooper, M.A., Poirier, G.G., Yang, P., and Weller, M.T. (2017) Hydroxylgugiaite: A new beryllium silicate mineral from the Larvik Plutonic Complex, Southern Norway and the Illmaussaq Alkaline Complex, South Greenland; the first member of the melilite group to incorporate a hydrogen atom. *Canadian Mineralogist*, 55, 219–232.
- Gross, S. (1977) The mineralogy of the Hatrurim Formation, Israel. *Geological Survey of Israel, Bulletin*, 70, 80.
- Hamada, M., and Akasaka, M. (2013) Distribution of cations at two tetrahedral sites in $\text{Ca}_2\text{MgSi}_2\text{O}_7$ – $\text{Ca}_2\text{Fe}^{3+}\text{AlSi}_2\text{O}_7$ series synthetic melilite and its relation to incommensurate structure. *Physics and Chemistry of Minerals*, 40, 259–270.
- Hanuza, J., Ptak, M., Mączka, M., Hermanowicz, K., Lorenc, J., and Kaminskii, A.A. (2012) Polarized IR and Raman spectra of $\text{Ca}_2\text{MgSi}_2\text{O}_7$, $\text{Ca}_2\text{ZnSi}_2\text{O}_7$ and $\text{Sr}_2\text{MgSi}_2\text{O}_7$ single crystals: Temperature-dependent studies of commensurate to incommensurate and incommensurate to normal phase transitions. *Journal of Solid State Chemistry*, 191, 90–101.
- Hawthorne, F.C., Uvarova, Y.A., and Sokolova, E. (2019) A structure hierarchy for silicate minerals: sheet silicates. *Mineralogical Magazine*, 83, 3–55.
- Hejny, C., Kahlenberg, V., Eberhard, T., and Krüger, H. (2016) Melilite-like modulation and temperature-dependent evolution in the framework structure of $\text{K}_2\text{Sc}[\text{Si}_2\text{O}_6]\text{F}$. *Acta Crystallographica*, B72, 209–222.
- Ito, J., and Hafner, S.S. (1974) Synthesis and study of gadolinites. *American Mineralogist*, 59, 700–708.
- Kabsch, W. (2010) Integration, scaling, space-group assignment and post-refinement. *Acta Crystallographica*, D66, 133–144.
- Kaiser, J., and Jeitschko, W. (2002) Crystal structure of the new barium zinc silicate $\text{Ba}_2\text{ZnSi}_2\text{O}_7$. *Zeitschrift für Kristallographie—New Crystal Structures*, 217, 25–26.
- Kimata, M. (1983a) The structural properties of synthetic Sr-åkermanite, $\text{Sr}_2\text{MgSi}_2\text{O}_7$. *Zeitschrift für Kristallographie—Crystalline Materials*, 163, 295–304.
- (1983b) The crystal structure and stability of Co-åkermanite, $\text{Ca}_2\text{CoSi}_2\text{O}_7$, compared with the mineralogical behaviour of Mg cation. *Neues Jahrbuch für Mineralogie Abhandlungen*, 146, 221–241.
- (1984) The structural properties of synthetic Sr-gehlenite, $\text{Sr}_2\text{Al}_2\text{Si}_2\text{O}_7$. *Zeitschrift für Kristallographie*, 167, 103–116.
- Kimata, M., and Ii, N. (1981) The crystal structure of synthetic åkermanite, $\text{Ca}_2\text{MgSi}_2\text{O}_7$. *Neues Jahrbuch für Mineralogie, Monatshefte*, 1981, 1–10.
- Kimata, M., and Ii, N.I. (1982) The structural property of synthetic gehlenite, $\text{Ca}_2\text{Al}_2\text{Si}_2\text{O}_7$. *Neues Jahrbuch für Mineralogie, Abhandlungen*, 144, 254–267.
- Kusaka, K., Ohmura, M., Hagiya, K., Iishi, K., and Haga, N. (1998) On variety of the Ca coordination in the incommensurate structure of synthetic iron-bearing åkermanite, $\text{Ca}_2(\text{Mg}_{0.55}\text{Fe}_{0.45})\text{Si}_2\text{O}_7$. *Mineralogical Journal*, 20, 47–58.
- Krzatula, A., Panikarovskii, T.L., Galuskin, I.O., and Galuskin, E.V. (2018) Dynamic disorder of Fe^{3+} ions in the crystal structure of natural barioferrite. *Minerals*, 8, 340.
- Krzatula, A., Krüger, B., Galuskin, I., Vapnik, Y., and Galuskin, E. (2020) Walstromite, $\text{BaCa}(\text{Si}_3\text{O}_8)_2$, from rankinite paravala within gehlenite hornfels of the Hatrurim Basin, Negev Desert, Israel. *Minerals*, 10, 407.
- Louisnathan, S.J. (1969) Refinement of the crystal structure of hardystonite, $\text{Ca}_2\text{ZnSi}_2\text{O}_7$. *Zeitschrift für Kristallographie Kristallographie*, 130, 427–437.
- (1970) The crystal structure of synthetic soda melilite, $\text{CaNaAlSi}_2\text{O}_7$. *Zeitschrift für Kristallographie*, 131, 314–321.
- (1971) Refinement of the crystal structure of a natural gehlenite, $\text{Ca}_2\text{Al}(\text{Al},\text{Si})_2\text{O}_7$. *Canadian Mineralogist*, 10, 822–837.
- Lyalina, L.M., Kadyrova, G.I., Selivanova, E.A., Zolotarev, A.A. Jr., Savchenko, Y.E., and Panikarovskii, T.L. (2019) On composition of meliphanite from nepheline syenite pegmatite of the Sakharjok Massif, Kola Peninsula. *Geology of Ore Deposits*, 61, 671–679.
- Malinovskii, Y.A., Pobedimskaya, E.A., and Belov, N.V. (1976) Synthesis and X-ray analysis of two new iron-containing barium germanates $\text{Ba}_2\text{FeGe}_2\text{O}_7$ and $\text{Fe}_2\text{NaBa}_6\text{Ge}_2\text{O}_{24}(\text{OH},\text{H}_2\text{O})$. *Kristallografiya*, 21, 1195–1197.
- Matsubara, S., Miyawaki, R., Kato, A., Yokoyama, K., and Okamoto, A. (1998) Okayamalite, $\text{Ca}_2\text{B}_2\text{Si}_2\text{O}_7$, a new mineral, boron analogue of gehlenite. *Mineralogical Magazine*, 62, 703–706.
- Medenbach, O., and Shannon, R.D. (1997) Refractive indices and optical dispersion of 103 synthetic and mineral oxides and silicates measured by a small-prism technique. *Journal of the Optical Society of America B*, 14, 3299–3318.
- Minster, T., Yoffe, O., Nathan, Y., and Flexer, A. (1997) Geochemistry, mineralogy, and paleoenvironments of deposition of the Oil Shale Member in the Negev. *Israel Journal of Earth Sciences*, 46, 41–59.
- Moore, P.B., and Louisnathan, S.J. (1967) Fresnoite: Unusual titanium coordination. *Science*, 156, 1361–1362.
- (1969) The crystal structure of fresnoite, $\text{Ba}_2(\text{TiO})\text{Si}_2\text{O}_7$. *Zeitschrift für Kristallographie—Crystalline Materials*, 130, 438–448.
- Murashko, M.N., Chukanov, N.V., Mukhanova, A.A., Vapnik, E., Britvin, S.N., Polekhovsky, Y.S., and Ivakin, Y.D. (2011) Barioferrite $\text{BaFe}_{12}\text{O}_{19}$: A new mineral species of the magnetoplumbite group from the Hatrurim Formation in Israel. *Geology of Ore Deposits*, 53, 558–563.
- Novikov, I., Vapnik, Y., and Safonova, I. (2013) Mud volcano origin of the Mottled Zone, South Levant. *Geoscience Frontiers*, 4, 597–619.
- Peng, C.-J., Tsao, R.-L., and Chou, Z.-R. (1962) Gugiaite, $\text{Ca}_2\text{BeSi}_2\text{O}_7$, a new beryllium mineral and its relation to the melilite group. *Scientia Sinica*, 11, 977–988.
- Peretyazhko, I.S., Savina, E.A., Khromova, E.A., Karmanov, N.S., and Ivanov, A.V. (2018) Unique clinkers and paralavas from a New Nyalga Combustion Metamorphic Complex in Central Mongolia: Mineralogy, geochemistry, and genesis. *Petrology*, 26, 181–211.
- Robinson, K., Gibbs, G.V., and Ribbe, P.H. (1971) Quadratic elongation: A quantitative measure of distortion in coordination polyhedra. *Science*, 172, 567–570.
- Sahama, T.G., Siivola, J., and Rehtijärvi, P. (1973) Andremerite, a new barium iron silicate, from Nyiragongo, Zaire. *Bulletin of the Geological Society of Finland*, 45, 1–8.
- Sale, M., Xia, Q., Avdeev, M., and Ling, C.D. (2019) Crystal and magnetic structures of melilite-type $\text{Ba}_2\text{MnSi}_2\text{O}_7$. *Inorganic Chemistry*, 58, 4164–4172.
- Seifert, F., Czank, M., Simons, B., and Schmahl, W. (1987) A commensurate-incommensurate phase transition in iron-bearing åkermanites. *Physics and Chemistry of Minerals*, 14, 26–35.
- Seryotkin, Y.V., Sokol, E.V., and Kokh, S.N. (2012) Natural pseudowollastonite: Crystal structure, associated minerals, and geological context. *Lithos*, 134–135, 75–90.
- Sharma, S.K., Simons, B., and Yoder, H.S. (1983) Raman study of anorthite, calcium Tschermak's pyroxene, and gehlenite in crystalline and glassy states. *American Mineralogist*, 68, 1113–1125.
- Sharygin, V.V., Lazic, B., Armbruster, T.M., Murashko, M.N., Wirth, R., Galuskin, I.O., Galuskin, E.V., Vapnik, Y., Britvin, S.N., and Logvinova, A.M. (2013) Shulamitite $\text{Ca}_2\text{TiFe}^{2+}\text{AlO}_6$ —A new perovskite-related mineral from Hatrurim Basin, Israel. *European Journal of Mineralogy*, 25, 97–111.
- Sharygin, V.V., Vapnik, Y., Sokol, E.V., Kamenetsky, V.S., and Shagam, R. (2006) Melt inclusions in minerals of schorlomite-rich veins of the Hatrurim Basin, Israel: Composition and homogenization temperatures. In P. Ni and Z. Li, Eds., *ACROFI I, Program with Abstracts*, p. 189–192.
- Sheldrick, G.M. (2008) A short history of SHELX. *Acta Crystallographica*, A64, 112–122.
- Shimizu, M., Kimata, M., and Iida, I. (1995) Crystal structure of $\text{Ba}_2\text{MgSi}_2\text{O}_7$ melilite: The longest tetrahedral MgO distance. *Neues Jahrbuch für Mineralogie Abhandlungen*, 170, 39–47.
- Sokol, E., Novikov, I., Zateeva, S., Vapnik, Y., Shagam, R., and Kozmenko, O. (2010) Combustion metamorphism in the Nabi Musa dome: new implications for a mud volcanic origin of the Mottled Zone, Dead Sea area. *Basin Research*, 22, 414–438.
- Sokol, E.V., Kozmenko, O.A., Kokh, S.N., and Vapnik, Y. (2012) Gas reservoirs in the Dead Sea area: evidence from chemistry of combustion metamorphic rocks in Nabi Musa fossil mud volcano. *Russian Geology and Geophysics*, 53, 745–762.
- Sokol, E.V., Seryotkin, Y.V., Kokh, S.N., Vapnik, Y., Nigmatulina, E.N., Goryainov, S.V., Belogub, E.V., and Sharygin, V.V. (2015) Flamite, $(\text{Ca},\text{Na},\text{K})_2(\text{Si},\text{P})\text{O}_6$, a new mineral from ultrahigh temperature combustion metamorphic rocks, Hatrurim Basin, Negev Desert, Israel. *Mineralogical Magazine*, 79, 583–596.
- Solovova, I.P., Girmis, A.V., Ryabchikov, I.D., and Simakin, S.G. (2006) High-temperature carbonatite melt and its interrelations with alkaline magmas of the Dunkel' dyk Complex, southeastern Pamirs. *Doklady Earth Sciences*, 410, 1148–1151.
- Stoe and Cie (2002) X-Area. Stoe and Cie, Darmstadt, Germany.
- Swainson, I.P., Dove, M.T., Schmahl, W.W., and Putnis, A. (1992) Neutron powder diffraction study of the åkermanite-gehlenite solid solution series. *Physics and Chemistry of Minerals*, 19, 185–195.
- Tovar, M., Dinnebier, R.E., and Eysel, E. (1998) The Cu(II) tetrahedron in åkermanite structure. *Materials Science Forum*, 278–281, 750–755.
- Vapnik, Y., Sokol, E., Murashko, M., and Sharygin, V. (2006) The enigma of Hatrurim. *Mineralogical Almanac*, 10, 69–77.
- Vapnik, Y., Sharygin, V.V., Sokol, E.V., and Shagam, R. (2007) Paralavas in a combustion metamorphic complex Hatrurim Basin, Israel. In G.B. Stracher, Ed., *Geology of Coal Fires, Case Studies from Around the World*. Geological Society of America.
- Wiedenmann, D., Zaitsev, A.N., Britvin, S.N., Krivovichev, S.V., and Keller, J. (2009) Alunoferrite, $(\text{Ca},\text{Na})_2(\text{Al},\text{Mg},\text{Fe}^{2+})(\text{Si}_2\text{O}_7)_2$, a new mineral from the active carbonatite-nephelinite-phonolite volcano Oldoinyo Lengai, northern Tanzania. *Mineralogical Magazine*, 73, 373–384.
- Yang, Z., Fleck, M., Pertlik, F., Tillmanns, E., and Tao, K.J. (2001) The crystal structure of natural gugiaite, $\text{Ca}_2\text{BeSi}_2\text{O}_7$. *Neues Jahrbuch für Mineralogie, Monatshefte*, 186–192.

MANUSCRIPT RECEIVED AUGUST 10, 2020

MANUSCRIPT ACCEPTED JANUARY 2, 2021

MANUSCRIPT HANDLED BY PAOLO LOTTI

Endnote:

¹Deposit item AM-22-17747, Online Materials. Deposit items are free to all readers and found on the MSA website, via the specific issue's Table of Contents (go to http://www.minsocam.org/MSA/ammin/TOC/2022/Jan2022_data/Jan2022_data.html). The CIF has been peer reviewed by our Technical Editors.